Protein NMR Spectroscopy at 150 kHz Magic-Angle Spinning Continues To Improve Resolution and Mass Sensitivity

Maarten Schledorn[+],[a] Alexander A. Malär[+],[a] Anahit Torosyan[+],[a] Susanne Penzel,[a] Daniel Klose,[a] Andres Oss,[b] Mai-Liis Org,[b] Shishan Wang,[c] Lauriane Lecoq,[c] Riccardo Cadalbert,[a] Ago Samoson,*[b] Anja Böckmann,*[c] and Beat H. Meier*[a]

Spectral resolution is the key to unleashing the structural and dynamic information contained in NMR spectra. Fast magic-angle spinning (MAS) has recently revolutionized the spectroscopy of biomolecular solids. Herein, we report a further remarkable improvement in the resolution of the spectra of four fully protonated proteins and a small drug molecule by pushing the MAS rotation frequency higher (150 kHz) than the more routinely used 100 kHz. We observed a reduction in the average homogeneous linewidth by a factor of 1.5 and a decrease in the observed linewidth by a factor 1.25. We conclude that even faster MAS is highly attractive and increases mass sensitivity at a moderate price in overall sensitivity.

Introduction

The knowledge of the three-dimensional structure of a protein is an essential first step to understanding its biomolecular function. In addition, it is vital for interfering with it, for example in the context of drug development. Solid-state NMR plays an important role in *de novo* 3D structure determination of particular protein classes, such as amyloids.[1–5] The method allows conformational details to be studied with particularly high sensitivity,[6–8] and can, for example, identify drug-binding sites or characterize dynamic features.[9–15]

Information content of the NMR spectrum increases with improved spectral resolution. For solid-state NMR, such resolution requires mechanical rotation of the sample around a fixed axis with respect to the magnetic field, known as magic-angle spinning (MAS).[16,17] Until very recently, most applications in biomolecular solid-state NMR have been based on carbon-13 detection because proton resonances were spectrally not sufficiently resolved. This was principally caused by insufficient averaging of large ^{1}H-^{1}H dipole interactions by MAS. However, with MAS frequencies approaching and exceeding 100 kHz, the linewidth for fully protonated proteins is reduced to a degree that makes proton-detected solid-state NMR an attractive alternative to carbon-13 detection.[18–29] Of course this holds true also for deuterated proteins that were back-exchanged to protons at exchangeable sites.

When comparing a 3.2 mm rotor (standard for ^{13}C-detected experiments on proteins with about 50 mg of sample) to a 0.7 mm rotor (for ^{1}H with about 0.5 mg sample), proton detection has the important advantage of reducing the required sample amount at comparable sensitivity by roughly two orders of magnitude, due to the narrowing of proton lines at faster spinning and the higher gyromagnetic ratio.[26,30,31] Further increases in spinning frequencies are expected to bring additional spectral resolution.[32,33] However, this obvious trend is countered by a considerable engineering complexity required to handle sample containment in a sub-millimeter range at the limit of mechanical rupture.

We here present experimental data recorded at 150 kHz MAS with a prototype 0.5 mm triple-resonance MAS probe (NMR Instituut, Tallinn, Estonia), for four representative proteins: the microcrystalline model protein ubiquitin (8.6 kDa), the archaeal RNA polymerase subunits 4 and 7 protein complex (Rpo4/7, 33.5 kDa), the prion domain of HET-s in its amyloid form (HET-s(218–289), 7.8 kDa, monomer weight), and the hepatitis-B viral capsid core protein (Cp149, 16.9 kDa × 240). We also investigated a small drug molecule as an organic reference structure for a many-spin system. The data show that the predicted improvements in spectral resolution and relaxation rate constants can be realized with increasing spinning frequencies, up to 150 kHz and predictably beyond, and that resulting gains in the signal-to-noise ratio (SNR) compensate for the scaling loss.

[a] *Dr. M. Schledorn,[+] A. A. Malär,[+] Dr. A. Torosyan,[+] Dr. S. Penzel, Dr. D. Klose, R. Cadalbert, Prof. Dr. B. H. Meier*
Physical Chemistry, ETH Zürich
8093 Zürich (Switzerland)
E-mail: beme@ethz.ch
[b] *A. Oss, M.-L. Org, Dr. A. Samoson*
Institute of Health Technologies, Tallinn University of Technology
Akadeemia tee 15a, 12618 Tallinn (Estonia)
E-mail: ago.samoson@ttu.ee
[c] *Dr. S. Wang, Dr. L. Lecoq, Dr. A. Böckmann*
Institut de Biologie et Chimie des Protéines
MMSB UMR 5086 CNRS/Université de Lyon, Labex Ecofect
7 passage du Vercors, 69367 Lyon (France)
E-mail: a.bockmann@ibcp.fr
[+] *These authors contributed equally to this work.*

Supporting information for this article is available on the WWW under https://doi.org/10.1002/cbic.202000341

Resolution and sensitivity considerations

The smaller the linewidth the better, at a fixed static magnetic field, the spectral resolution. For the fast spinning limit the resolution increases linearly with spinning frequencies which, with current technology requires to linearly decrease the rotor diameter d (see, e.g., the review in ref. [32]). We assume here a uniform scaling of the dimensions of the rotor and of the coil by a factor $\kappa = d/d_r$ that describes the ratio of the rotor diameter d with respect to the reference rotor with diameter d_r. The rotor length is assumed to scale by the same factor κ. We assume for the following discussion that $\kappa < 1$ (the reference rotor is always the larger of the two) and, for simplicity assume that the rotor walls are infinitely thin. The fact that the two rotors to be compared need to be completely full with sample is obvious, but not trivial in practice. Notes on sample filling are made in the closing paragraph of the Sample Preparation section of the Supporting Information.

Comparing a 0.7 mm rotor to a 3.2 mm yields $\kappa \approx 0.22$. The sensitivity $\sigma = S/S_r$ of the experiment as a function of κ depends on a number of factors, such as the sensitivity change by the sample volume (σ_V), the coil sensitivity (σ_{coil}), and so forth. S denotes the peak amplitude of the NMR signal from the considered rotor, and S_r represents the peak amplitude from the reference rotor. The sample volume and therefore the number of spins scales as κ^3 and provides a factor of $\sigma_V = \kappa^3$ to the total sensitivity. Note that we have assumed here that the rotor length also scales with κ; if the length could be kept constant for the two rotors compared, which seems to be difficult in practice, the signal loss would only be $\sigma_V = \kappa^2$. Furthermore, detection with optimized smaller coils (fitting the rotor diameter) increases the sensitivity per unit volume (the mass sensitivity) by a factor of approximately $\sigma_{coil} = \kappa^{-1}$. We note that this is a rough estimation and the actual value depends on the details of the circuits. To compensate the resulting geometry-related signal loss (for samples that are not mass-limited in the sense that the amount of protein available is not a limiting factor) of $\sigma_V \sigma_{coil} = \kappa^2$ as much as possible, further signal gains need to be achieved by increased spinning frequencies. Two factors are involved: i) a decrease in proton linewidths (σ_{MAS}), and ii) a gain in polarization-transfer efficiencies (σ_{PT}).

The total proton linewidth (Δ^{tot}) can be described by two different contributions, a homogeneous and an inhomogeneous one: $\Delta^{tot}(\nu_r) = \Delta^{homo}(\nu_r) + \Delta^{inhomo}$.[34] One should mention that Δ^{homo} in turn is composed by coherent, incoherent and exchange contributions: $\Delta^{homo}(\nu_r) = \Delta^{coh}(\nu_r) + \Delta^{incoh}(\nu_r) + \Delta^{exchange}$, where the coherent contribution, representing the incompletely averaged dipole interactions, is found to be dominant for well-ordered and rigid samples: $\Delta^{homo}(\nu_r) \cong \Delta^{coh}(\nu_r)$.[35,36] In the following, we neglect possible contributions from chemical exchange (as discussed, e.g., by Marion and colleagues[37]). The ratio of the proton homogeneous linewidths at two different spinning frequencies is, to first approximation, inversely proportional to the ratio of the spinning frequencies which, in turn, are proportional to κ: $\sigma_{MAS} = \frac{\Delta^{coh}(\nu)}{\Delta^{coh}(\nu_r)} = \kappa^{-1}$.[36] In summary, for samples where the homogeneous contribution dominates the total linewidth, the predicted NMR sensitivity is expected to scale linearly with the rotor dimensions $\sigma_{MAS}\sigma_V\sigma_{coil} = \kappa$.

Lastly, the polarization- and coherence-transfer processes during the NMR experiment have efficiencies that depend on the relaxation-rate constants R_2' and $R_{1\rho}$, which both are known to become smaller with faster spinning.[38,39] It has been demonstrated that the polarization-transfer efficiency at 90 kHz MAS is roughly between 0.20 and 0.90 for each transfer step[28] resulting, for experiments showing multiple transfers, in low overall efficiencies, often below 0.10, for example, 0.03 for an hcocaCBcacoNH 3D experiment[28] including seven polarization-transfer steps. Improved polarization transfer at faster MAS thus has immense potential to enhance global sensitivity, notably in high-dimensional spectra,[40] which contain multiple transfer steps and will profit correspondingly stronger. Ideally the gain can be $\sigma_{PT} = \kappa^{-1}$ or higher in which case the absolute signal of the smaller rotor exceeds the one from the larger rotor if both rotate at their maximum frequency: $\sigma_{PT}\sigma_{MAS}\sigma_V\sigma_{coil} > 1$, whereas $\kappa < 1$.

Results and Discussion

Multidimensional protein spectra recorded at 150 kHz MAS

Using a 0.5 mm triple-resonance MAS probe, we recorded a set of proton-detected spectra (hNH, hCH, hCANH) on different proteins. Figure 1 shows the 2D and 3D spectra (see also Figure S1) of a fully protonated protein complex of Rpo4 and Rpo7 (Rpo4/7), in which only Rpo7 is uniformly $^{13}C/^{15}N$-labeled and therefore visible in our spectra. Although frictional heating was significant (30 °C without external cooling), the cooling system allowed to stabilize the sample temperature at approximately 10 °C (Figure S2). The resonance assignment has been reported.[41] The spectra provide a complete fingerprint of the protein, as they display all its backbone ^1H, ^{13}C and ^{15}N resonances, with the exception of the prolines. The hNH 2D spectrum, given in Figure 1A, predominantly shows backbone-nitrogen to amide-proton (H^N) correlations that are then additionally correlated to the backbone Cα resonances in a 3D hCANH spectrum, shown in a set of planes in Figure 1B. Resolved Hα-Cβ and Hβ-Cα crosspeaks are visible in the 2D hCH Figure 1C; some further aliphatic side-chain crosspeaks are also observed. Experimental parameters can be found in the Materials and Methods in the Supporting Information and Table S1.

Linewidth and sensitivity improve with faster MAS using same rotor size

The spinning-frequency dependence of the linewidths is illustrated by comparing hNH spectra of Rpo4/7 recorded at 100 and 150 kHz in Figure 2. From the stack plots in Figure 2A and B it becomes immediately appreciable that the total linewidth reduces, whereas peak amplitudes concomitantly

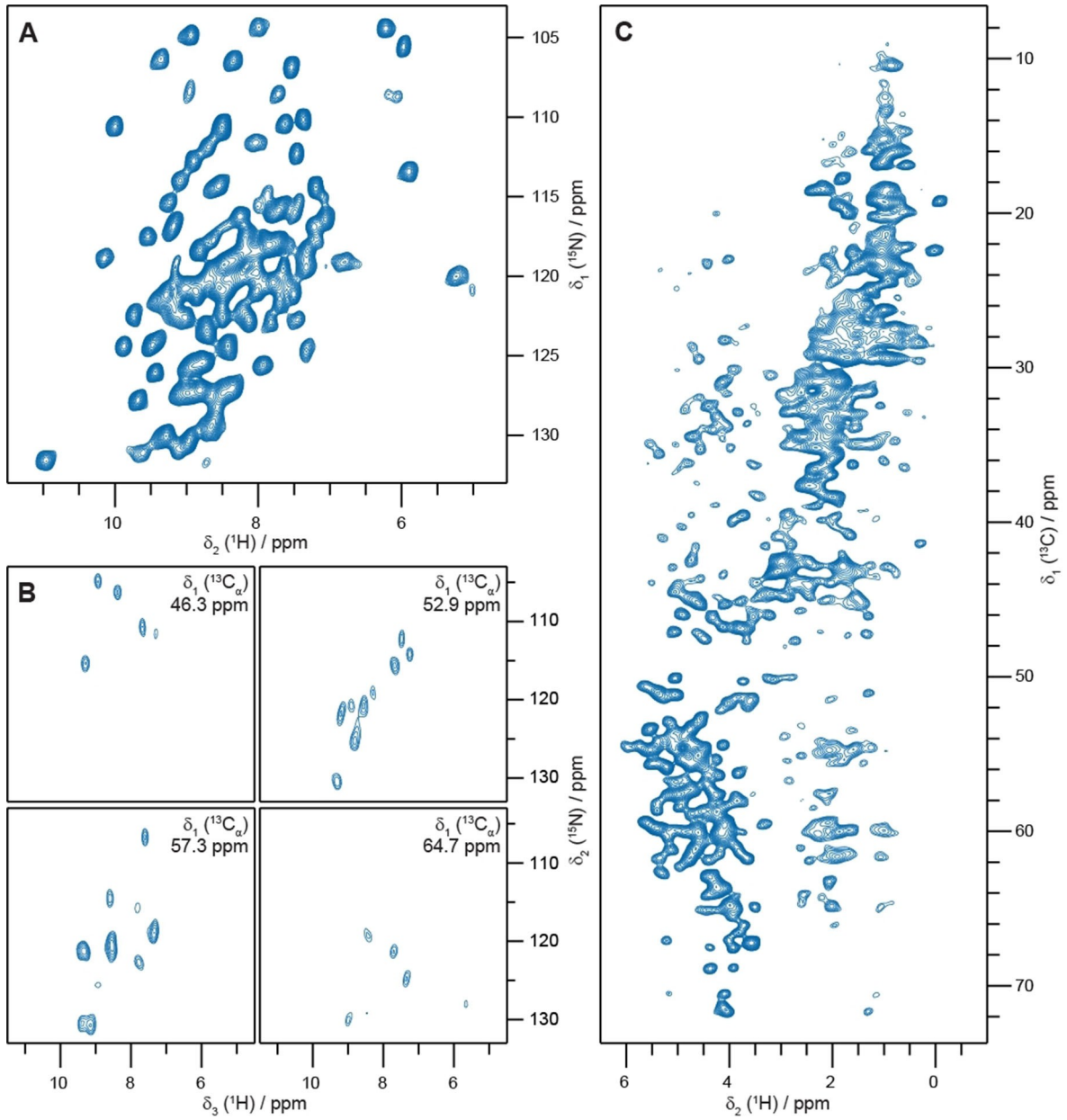

Figure 1. 2D and 3D heteronuclear correlation spectra of the Rpo4/7 complex recorded at 150 kHz MAS. A) hNH correlation spectrum processed with a QSINE 4 apodization function and cutoff just above the noise level. B) Representative planes from a hCANH 3D spectrum (cf. Figure S1 for further details). C) hCH 2D correlation spectrum with crosspeaks to Hα, Hβ, and further aliphatic protons (aromatic region of the spectrum not shown).

increase at faster spinning. Overlays of the 100 and 150 kHz MAS spectra as contour plots are given in (Figure 2C) with the assignment[41] of the peaks that were analyzed residue-specifically with respect to sensitivity. We observe an average increase in signal intensity by a factor $\sigma^{exp} = 1.5 \pm 0.2$ when MAS increases from 100 to 150 kHz (Figure 2F). This improvement can be due to both line-narrowing (σ_{MAS}) and higher transfer efficiencies (σ_{PT}): $\sigma^{exp} = \sigma_{MAS}\sigma_{PT}$. For all peaks labeled in Figure 2C, some of which are illustrated with traces in Figure 2D, we observe a mean linewidth decrease by 36 ± 8 Hz (from 193 ± 7 to 157 ± 4 Hz), which corresponds to a reduction in linewidth by a factor of 1.23 ± 0.05. This indicatates that half of the gain in intensity (1.5) is obtained from the reduction of the linewidth, leaving the other half to be improvement of the cross-polarization transfer. The improvement in cross-polarization intensity (Figure S3) is not necessarily expected but seems to be found also in other systems. It is the subject of further investigation.

Sensitivity considerations between rotor sizes

The measurements at 100 kHz described above could have been done in a 0.7 mm instead of 0.5 mm probe, increasing the

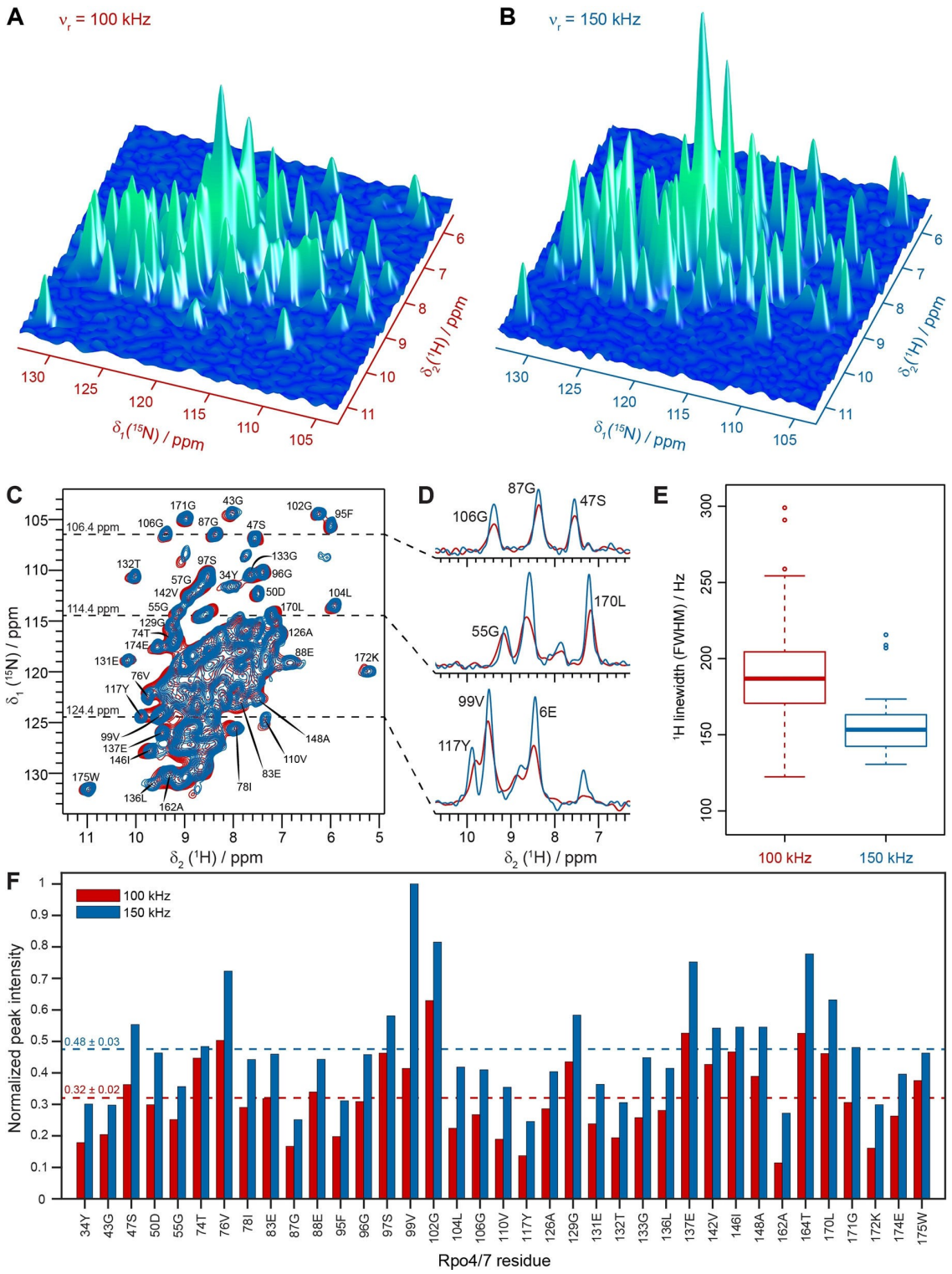

Figure 2. Comparison of resolution and signal intensity for an hNH correlation spectrum of Rpo4/7 at 100 and 150 kHz MAS. A) and B) 3D plots of 2D correlation experiments recorded at 100 and 150 kHz MAS, respectively. Spectra are plotted at the same absolute intensity scale and were obtained, in a back-to-back measurement, in the 0.5 mm probe, with identical acquisition and processing parameters, except for the spin-lock fields matching the two different MAS frequencies. C) Overlay of the spectra as contour plot. The peaks that are indicated with an assignment label in (C) were used for site-specific relaxation analysis (Figure 4). D) 1D extracts, with 100 kHz in red and 150 kHz in blue. E) Summary of the corresponding linewidths of the 37 labeled peaks in (C) as boxplots, indicating the minimum and maximum linewidths, the first and third quartile (forming the interquartile range), and the median values indicated by the thick lines at 187 and 153 Hz. Outliers were defined as more than 1.5 times the interquartile range above the third quartile. Mean linewidths (not indicated in the boxplots) are 193 ± 7 and 157 ± 4 Hz, at 100 and 150 kHz MAS, respectively. F) Site-specific signal intensity at both MAS frequencies. All peak intensities are normalized to the most intensive peak (99 V at 150 kHz), with mean normalized peak intensities indicated as dashed lines at 0.32 ± 0.02 (100 kHz) and 0.48 ± 0.03 (150 kHz), corresponding to an intensity gain of a factor 1.48 ± 0.13 for 150 compared to 100 kHz MAS.

diameter by a factor $\kappa = 1.4$ and the sample volume by a factor $\kappa = 2.7$ theoretically, and about 1.9 in our setup (where, e.g., the rotor walls are not infinitely thin; cf. sample volumes below). Therefore, we experimentally compared full 0.7 and 0.5 mm rotors with uniformly $^{13}C/^{15}N$-labeled capsids of the hepatitis B virus (HBV) core protein Cp149[7,26] in their respective probes at 100 and 150 kHz MAS (Figure S4 and Table S2). We note that additional factors like different probe efficiencies for the two probe heads used can influence this comparison. At 150 kHz MAS, in a 0.5 mm rotor, we find an SNR/$\sqrt{h}$ reduced by a factor $\sigma^{exp} = 0.66 \pm 0.09$ when compared to a 0.7 mm rotor at 100 kHz, despite the reduction of sample volume by a factor of $\sigma_V = 0.52$ (0.59 vs. 0.31 μL volumes). This clearly indicates that the higher coil efficiency, the line narrowing and improvements in polarization-transfer efficiency indeed increase the mass sensitivity by: $\sigma_{coil}\sigma_{MAS}\sigma_{PT} = 1.27 \pm 0.17$.

Table 1. Parameters describing the spinning-frequency dependence of the homogeneous linewidth for a range of MAS frequencies from 90 to 150 kHz (Figure 3). Values at zero (without error bars) were fixed in the respective evaluation (see also Table S3). Errors are given as 2σ, roughly equivalent to the 95% confidence intervals drawn as dashed lines in Figure 3.

	$\Delta^{homo}(\nu_r) = c^{(1)} + c^{(2)}/\nu_r + c^{(3)}/\nu_r^2$		
	$c^{(1)}$ [Hz]	$c^{(2)}$ [kHz^2]	$c^{(3)}$ [kHz^3]
Rpo4/7	−01 ± 10	14 ± 1	0
HET-s (218–289)	0–8 ± 9	15 ± 1	0
Cp149	−09 ± 10	13 ± 1	0
ubiquitin	−13 ± 25	14 ± 3	0
meldonium NH	0	13 ± 5	4.0 ± 0.6
meldonium CH_3	0	12 ± 1	1.1 ± 0.2
meldonium CH_2	0	47 ± 4	0.7 ± 0.5

Bulk coherence lifetimes increase with faster MAS frequencies

We investigated the amide–proton proton bulk homogeneous linewidths $\Delta^{homo}(\nu_r) = 1/\pi T_2'$, an average over all residues, by Hahn echo transverse relaxation experiments in four different fully protonated proteins. Although bulk data are obviously less informative than site-specific data, they have the advantage that they can be measured in a short experiment. The values for Rpo4/7 are given in Figure 3A, over a MAS-frequency range of 90–150 kHz, according to $\Delta^{homo}(\nu_r) = c^{(1)} + c^{(2)}/\nu_r + c^{(3)}/\nu_r^2$. As expected for the fast-spinning regime, the linewidth decreases linearly with the inverse of the MAS frequency $\Delta^{homo}(\nu_r) = c^{(2)}/\nu_r$, with $c^{(2)} = 14 \pm 1$ kHz^2 for Rpo4/7. For HET-s (218–289), a fungal prion in its β-sheet-rich amyloid form,[1,42] we obtain $c^{(2)} = 15 \pm 1$ kHz^2 (Figure 3B), for Cp149 (Figure 3C) we find $c^{(2)} = 13 \pm 1$ kHz^2, and for microcrystalline ubiquitin (Figure 3D) $c^{(2)} = 14 \pm 3$ kHz^2. Site-specific data are presented below, but we note here that $c^{(2)}$ is remarkably similar for the NH region of all four fully protonated proteins investigated (Figure 3 and Table 1).

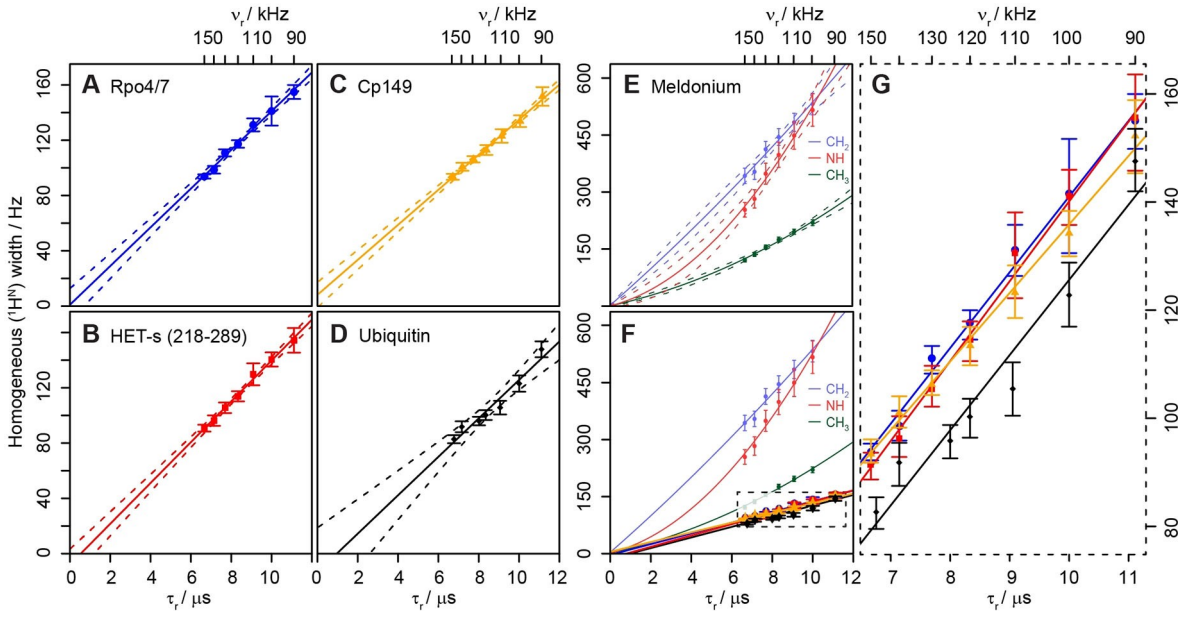

Figure 3. Bulk homogeneous linewidths of amide protons in a MAS range of 90 to 150 kHz are similar for various protein samples, but differ for meldonium protons. The fully protonated $^{13}C,^{15}N$-labeled samples of A) Rpo4/7, B) HET-s (218–289 s), C) human Cp149 capsids, and D) microcrystalline ubiquitin, can all be fitted by a linear function with a slope of 13–15 kHz^2, while intercepting the origin within a confidence interval of 95% (indicated by dashed lines above and below each fit). E) In contrast, the homogeneous linewidth for meldonium CH_2, NH, and CH_3 groups decreases much faster for shorter rotor periods and a significant quadratic component is observed. At the same time, the homogeneous broadening in general is much stronger than for protein amide protons; this can be explained by stronger proton–proton couplings resulting from the molecular structure of the small compound as well as from the chemical-shift differences (see also Figure 5). F) All samples in relation to each other. G) Expansion of the dashed box in (F) to distinguish the various protein samples that are very similar in slope and intercept. Colors in (G) correspond to those in (A)–(D).

Site-specific homogeneous linewidths improve for all protein residues

To go beyond the bulk linewidths, we extracted site-specific homogeneous linewidths from a selection of baseline-separated peaks of Rpo4/7 at MAS frequencies of 90, 120 and 150 kHz (Figure 4A). Consistently, the homogeneous linewidths decrease with increasing spinning frequency, as expected from the bulk behavior (Figure 3A). Δ^{homo} for the three data sets at 90, 120, and 150 kHz reaches a median value of 140 ± 10, 116 ± 5, and 90 ± 3 Hz, respectively. Interpolating these values to obtain the mean homogeneous linewidth at 100 kHz MAS gives 132 ± 6 Hz. The corresponding improvement factor from 100 to 150 kHz (132 ± 6 Hz/90 ± 3 Hz $=1.47\pm0.09$) corresponds to the predicted improvement based on a linear correlation between the ratio of the spinning frequencies.

The inhomogeneous contribution $\Delta^{inhomo}=\Delta^{tot}-\Delta^{homo}$ for Rpo4/7 (data at 150 kHz MAS) is given on a per-residue basis in Figure 4B, with a mean value of 76 ± 6 Hz, compared to a mean homogeneous contribution of 87 ± 3 Hz. Figure 4B also gives site-specific inhomogeneous contributions in HET-s (218–289) and Cp149. All three data sets in Figure 4B show a residue-

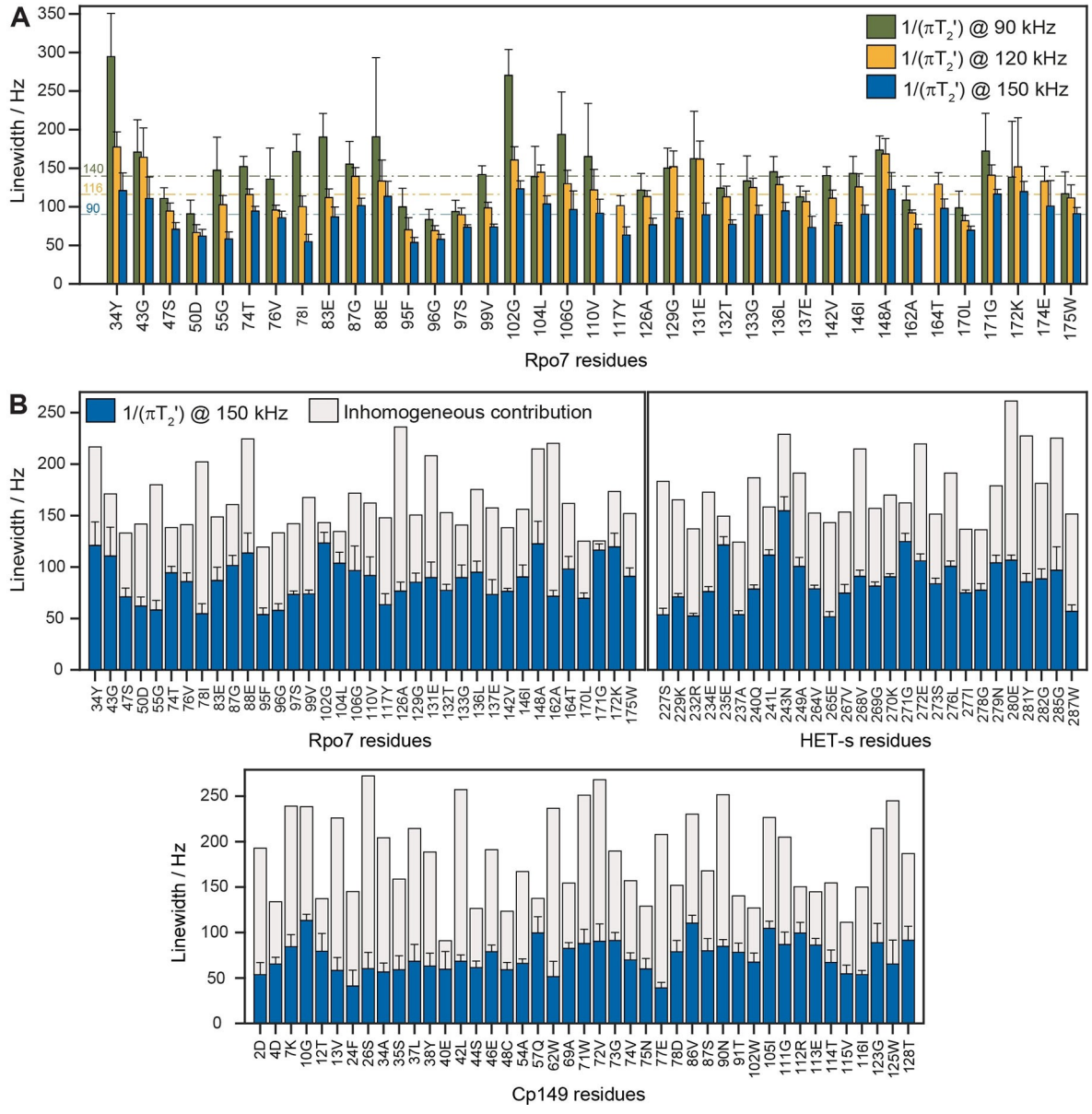

Figure 4. Protein-site-specific T_2' relaxation analyses for varying MAS frequencies. A) Relaxation data were recorded at three MAS frequencies in eight 2D spectra for each, with various delays. Peaks that were resolved in all 24 spectra (Figure 2C) were used for site-specific analysis, of which the result is expressed as $(\pi T_2')^{-1}$ [Hz], representing the homogeneous contribution. The three instances where a 90 kHz histogram bin is missing are troubled by peak overlap in the 2D spectrum and were consequently excluded from this figure. The shown error bars correspond to 2σ, where σ indicates the experimental error, and are symmetric to the negative side although not shown in this direction for graphic clarity. Median values for each of the three data sets are given as dashed lines, with the corresponding value in Hz toward the far left of the panel. B) Homogeneous and inhomogeneous linewidth contributions for Rpo4/7, HET-s (218–289), and Cp149 residues at 150 kHz MAS. Mean inhomogeneous contributions to the total linewidth are 45, 51, and 58% respectively.

dependent inhomogeneous contribution. We conclude that, for most residues, the dominant contribution to the linewidth still comes from coherent contributions, but the inhomogeneous contribution is of comparable magnitude, and even becomes larger for a number of residues in the HBV core protein. As the HBV capsid has four different molecules in the unit cell,[43] unresolved peak doubling[7,26] of the four expected signals might contribute to the inhomogeneous linewidth.

The drug molecule meldonium

We investigated the homogeneous linewidth of NH and CH_x protons of the organic drug molecule meldonium (Figure 3E and F), for which proton spectra and their assignment are given in Figure 5A.[44] In contrast to the investigated protein amide protons, meldonium protons show a very different correlation between homogeneous linewidth and MAS frequency, with linear fit components $c^{(2)} = 13 \pm 5$, 12 ± 1, and 47 ± 4 kHz^2 for NH, CH_3, and CH_2 values, respectively (Figure 3E), and with non-vanishing quadratic contributions $c^{(3)}$ (Tables 1 and S3), thus indicating significantly stronger proton–proton couplings. Although the spectral lines are thus significantly broader than the protein NH resonances at all spinning frequencies, their width decreases even more spectacularly with increasing spinning frequency (Figure 5A).

The homogeneous linewidth at 150 kHz for the three assigned proton resonances in the meldonium spectrum amounts to 340 ± 20 Hz for the CH_2 group; 121 ± 5 Hz for the CH_3; and 250 ± 20 Hz for the NH group (Figure 5B). In comparison, the fitted FWHM Δ^{tot} for each of these components is 660, 270, and 470 Hz, respectively (Figure 5C), thus indicating that also in this case, the homogeneous broadening still forms a substantial contribution to the linewidth. We note that in particular the CH_2 proton resonances are very broad and of relatively low amplitude compared to the 9:4 abundance of methyl to methylene protons, even at 150 kHz MAS. To verify that these broader lines are indeed caused by a stronger dipolar-coupling network, we calculated the coherent linewidths at this spinning frequency from the crystal structure[44] and the observed chemical shifts by using a second-moment approach.[35] We obtain homogeneous linewidths of 415 Hz for the CH_2, 228 Hz for the CH_3, and 398 Hz for the NH groups, thus indicating that the homogeneous line broadening is again the dominant contribution. The meldonium spectrum, expected to be representative for many drugs and dense spin networks, is thus predicted to particularly benefit from MAS frequencies beyond those presently realized. In fact, for some lines such as that of the CH_2 group (at $\delta_1 = 2.5$ ppm), the improved resolution due to faster MAS reveals a line that would otherwise be broadened completely beyond visibility.

Conclusion

In this work, we have presented protein NMR spectroscopy of fully protonated samples at 150 kHz MAS. Spectra of four proteins were recorded within experimental times and resulting SNR per $\sqrt{h}$ similar to 100 kHz experiments with respectively larger rotors. For the protein complex Rpo4/7, we found a linear improvement of homogeneous linewidths with the inverse spinning frequency in the range between 90 and 150 kHz MAS and a narrowing of the total linewidth from 193 ± 7 to 157 ± 4 Hz, improving by a factor 1.23 ± 0.05. The mass sensitivity increases by a factor of 1.27 ± 0.17.

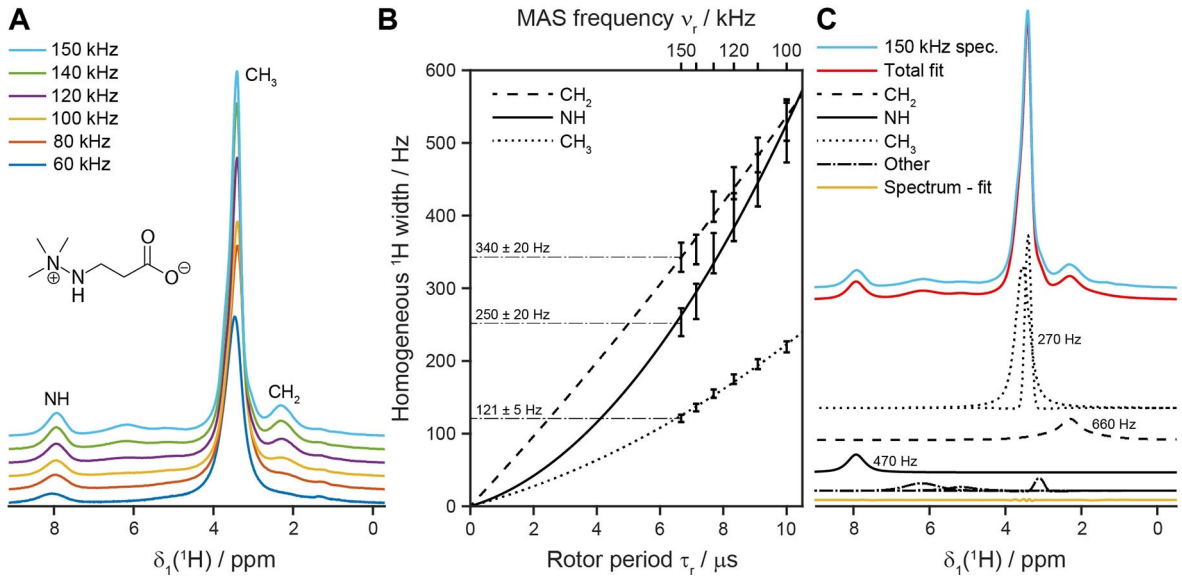

Figure 5. Resolution improvement in meldonium over the range 60–150 kHz MAS. A) 1D proton spectra at 60–150 kHz MAS, with assignment of the NH and triple CH_3 groups, as well as one of the CH_2 groups shown in the molecular structure of meldonium. B) Experimental homogeneous linewidths for the three assigned groups, with widths at 150 kHz (rotor period of 6.7 µs) of 340, 250, and 121 Hz, for CH_2, NH, and CH_3, respectively. C) FWHM fit of the three assigned groups in the 150 kHz 1D spectrum, performed with DMFIT.[45]

Our data demonstrate that biomolecular solid-state NMR spectroscopy can greatly benefit from MAS spinning frequencies beyond the presently often applied 100–111 kHz. The homogeneous linewidth of the backbone amide proton as a function of the spinning frequency shows a universal behavior for all four proteins investigated. Proton networks of strongly coupled spins with near-degenerate resonance frequencies, like the drug meldonium investigated here, but also CH_2 groups in proteins still exhibit remarkably broad lines, even at 150 kHz. However, their resolution also benefits considerably from increased MAS.

Author contributions

A.B. and B.H.M. designed the research, M.S., A.M., A.T. and S.P. performed the NMR experiments, M.S., A.M., A.T., S.P., A.B. and B.H.M. analyzed data, A.O., M.-L.O., and A.S. built the probe head. S.W. and L.L. prepared the Cp149 sample, A.T. and D.K. prepared the Rpo4/7 sample, R.C. prepared ubiquitin and HET-s (218–289). M.S., A.B. and B.H.M. wrote the manuscript with input from other authors who contributed to editing the manuscript and approved submission.

Acknowledgements

This research was supported by the Estonian Science Agency (PUT 1534), the French Agence Nationale de Recherche (A.B., ANR-14-CE09-0024B) and the LABEX ECOFECT (A.B., ANR-11-LABX-0048) within the Université de Lyon program Investissements d'Avenir (A.B., ANR-11-IDEX-0007), by the Swiss National Science Foundation (Grant 200020_159707), and by the European Research Council (ERC) under the European Union's Horizon 2020 research and innovation program (grant agreement no. 741863, FASTER).

Conflict of Interest

The authors declare no conflict of interest.

Keywords: fast MAS · proteins · solid-state NMR spectroscopy

[1] C. Wasmer, A. Lange, H. Van Melckebeke, A. B. Siemer, R. Riek, B. H. Meier, *Science* **2008**, *319*, 1523–1526.
[2] A. K. Schütz, T. Vagt, M. Huber, O. Y. Ovchinnikova, R. Cadalbert, J. Wall, P. Güntert, A. Böckmann, R. Glockshuber, B. H. Meier, *Angew. Chem. Int. Ed.* **2015**, *54*, 331–335; *Angew. Chem.* **2015**, *127*, 337–342.
[3] M. T. Colvin, R. Silvers, Q. Z. Ni, T. V. Can, I. Sergeyev, M. Rosay, K. J. Donovan, B. Michael, J. Wall, S. Linse, R. G. Griffin, *J. Am. Chem. Soc.* **2016**, *138*, 9663–9674.
[4] M. D. Tuttle, G. Comellas, A. J. Nieuwkoop, D. J. Covell, D. A. Berthold, K. D. Kloepper, J. M. Courtney, J. K. Kim, A. M. Barclay, A. Kendall, W. Wan, G. Stubbs, C. D. Schwieters, V. M. Y. Lee, J. M. George, C. M. Rienstra, *Nat. Struct. Mol. Biol.* **2016**, *23*, 409–415.
[5] M. A. Wälti, F. Ravotti, H. Arai, C. G. Glabe, J. S. Wall, A. Böckmann, P. Güntert, B. H. Meier, R. Riek, *Proc. Natl. Acad. Sci. USA* **2016**, *113*, E4976–E4984.
[6] S. D. Cady, T. V. Mishanina, M. Hong, *J. Mol. Biol.* **2009**, *385*, 1127–1141.
[7] L. Lecoq, S. Wang, T. Wiegand, S. Bressanelli, M. Nassal, B. H. Meier, A. Böckmann, *ChemPhysChem* **2018**, *19*, 1336–1340.
[8] R. Spadaccini, H. Kaur, J. Becker-Baldus, C. Glaubitz, *Biochim. Biophys. Acta Biomembr.* **2018**, *1860*, 833–840.
[9] K. Henzler-Wildman, D. Kern, *Nature* **2007**, *450*, 964–972.
[10] M. R. Elkins, J. K. Williams, M. D. Gelenter, P. Dai, B. Kwon, I. V. Sergeyev, B. L. Pentelute, M. Hong, *Proc. Natl. Acad. Sci. USA* **2017**, *114*, 12946–12951.
[11] C. M. Quinn, M. Wang, M. P. Fritz, B. Runge, J. Ahn, C. Xu, J. R. Perilla, A. M. Gronenborn, T. Polenova, *Proc. Natl. Acad. Sci. USA* **2018**, *115*, 11519–11524.
[12] A. K. Schütz, S. Hornemann, M. A. Wälti, L. Greuter, C. Tiberi, R. Cadalbert, M. Gantner, R. Riek, P. Hammarström, K. P. R. Nilsson, A. Böckmann, A. Aguzzi, B. H. Meier, *ACS Chem. Neurosci.* **2018**, *9*, 475–481.
[13] S. K. Vasa, H. Singh, P. Rovó, R. Linser, *J. Phys. Chem. Lett.* **2018**, *9*, 1307–1311.
[14] D. Lacabanne, C. Orelle, L. Lecoq, B. Kunert, C. Chuilon, T. Wiegand, S. Ravaud, J.-M. Jault, B. H. Meier, A. Böckmann, *Commun. Biol.* **2019**, *2*, 149.
[15] T. Wiegand, R. Cadalbert, D. Lacabanne, J. Timmins, L. Terradot, A. Böckmann, B. H. Meier, *Nat. Commun.* **2019**, *10*, 31.
[16] E. R. Andrew, A. Bradbury, R. G. Eades, *Nature* **1958**, *182*, 1659–1659.
[17] I. J. Lowe, *Phys. Rev. Lett.* **1959**, *2*, 285–287.
[18] M. J. Knight, A. L. Webber, A. J. Pell, P. Guerry, E. Barbet-Massin, I. Bertini, I. C. Felli, L. Gonnelli, R. Pierattelli, L. Emsley, A. Lesage, T. Herrmann, G. Pintacuda, *Angew. Chem. Int. Ed.* **2011**, *50*, 11697–11701; *Angew. Chem.* **2011**, *123*, 11901–11905.
[19] J. R. Lewandowski, J.-N. Dumez, Ü. Akbey, S. Lange, L. Emsley, H. Oschkinat, *J. Phys. Chem. Lett.* **2011**, *2*, 2205–2211.
[20] E. Barbet-Massin, A. J. Pell, J. S. Retel, L. B. Andreas, K. Jaudzems, W. T. Franks, A. J. Nieuwkoop, M. Hiller, V. Higman, P. Guerry, et al., *J. Am. Chem. Soc.* **2014**, *136*, 12489–12497.
[21] V. Agarwal, S. Penzel, K. Szekely, R. Cadalbert, E. Testori, A. Oss, J. Past, A. Samoson, M. Ernst, A. Böckmann, B. H. Meier, *Angew. Chem. Int. Ed.* **2014**, *53*, 12253–12256; *Angew. Chem.* **2014**, *126*, 12450–12453.
[22] L. B. Andreas, K. Jaudzems, J. Stanek, D. Lalli, A. Bertarello, T. Le Marchand, D. Cala-De Paepe, S. Kotelovica, I. Akopjana, B. Knott, S. Wegner, F. Engelke, A. Lesage, L. Emsley, K. Tars, T. Herrmann, G. Pintacuda, *Proc. Natl. Acad. Sci. USA* **2016**, *113*, 9187–9192.
[23] J. Stanek, L. B. Andreas, K. Jaudzems, D. Cala, D. Lalli, A. Bertarello, T. Schubeis, I. Akopjana, S. Kotelovica, K. Tars, et al., *Angew. Chem. Int. Ed.* **2016**, *55*, 15504–15509; *Angew. Chem.* **2016**, *128*, 15730–15735.
[24] T. Schubeis, T. Le Marchand, L. B. Andreas, G. Pintacuda, *J. Magn. Reson.* **2018**, *287*, 140–152.
[25] G. David, M.-L. Fogeron, M. Schledorn, R. Montserret, U. Haselmann, S. Penzel, A. Badillo, L. Lecoq, P. André, M. Nassal, R. Bartenschlager, B. H. Meier, A. Böckmann, *Angew. Chem. Int. Ed.* **2018**, *57*, 4787–4791; *Angew. Chem.* **2018**, *130*, 4877–4882.
[26] L. Lecoq, M. Schledorn, S. Wang, S. Smith-Penzel, A. A. Malär, M. Callon, M. Nassal, A. Böckmann, *Front. Mol. Biosci.* **2019**, *6*, 58.
[27] Y.-L. Lin, Y.-S. Cheng, C.-I. Ho, Z.-H. Guo, S.-J. Huang, M.-L. Org, A. Oss, A. Samoson, J. C. C. Chan, *Chem. Commun.* **2018**, *54*, 10459–10462.
[28] S. Penzel, A. A. Smith, V. Agarwal, A. Hunkeler, M.-L. Org, A. Samoson, A. Böckmann, M. Ernst, B. H. Meier, *J. Biomol. NMR* **2015**, *63*, 165–186.
[29] B. Reif, "Proton-Detection in Biological MAS Solid-State NMR Spectroscopy" in *Modern Magnetic Resonance* (Ed.: G. A. Webb), Springer, **2018**, pp. 879–910.
[30] A. Samoson, T. Tuherm, J. Past, A. Reinhold, I. Heinmaa, T. Anupõld, M. E. Smith, K. J. Pike, "Fast Magic-Angle Spinning: Implications" in *Encyclopedia of Magnetic Resonance*, Wiley, Chichester, **2010**.
[31] V. S. Mandala, M. Hong, *Curr. Opin. Struct. Biol.* **2019**, 58, 183–190.
[32] A. Böckmann, M. Ernst, B. H. Meier, *J. Magn. Reson.* **2015**, *253*, 71–79.
[33] A. Samoson, *J. Magn. Reson.* **2019**, *306*, 167–172.
[34] A. Abragam, *Principles of Nuclear Magnetism*, Oxford University Press, **1961**.
[35] A. A. Malär, S. Smith-Penzel, G.-M. Camenisch, T. Wiegand, A. Samoson, A. Böckmann, M. Ernst, B. H. Meier, *Phys. Chem. Chem. Phys., 21*, 18850–18865.
[36] S. Penzel, A. Oss, M.-L. Org, A. Samoson, A. Böckmann, M. Ernst, B. H. Meier, *J. Biomol. NMR* **2019**, *73*, 19–29.
[37] D. Marion, D. F. Gauto, I. Ayala, K. Giandoreggio-Barranco, P. Schanda, *ChemPhysChem* **2019**, *20*, 276–284.
[38] E. Brunner, D. Freude, B. C. Gerstein, H. Pfeifer, *J. Magn. Reson.* **1990**, *90*, 90–99.

[39] U. Sternberg, R. Witter, I. Kuprov, J. M. Lamley, A. Oss, J. R. Lewandowski, A. Samoson, *J. Magn. Reson.* **2018**, *291*, 32–39.
[40] H. W. Orton, J. Stanek, T. Schubeis, D. Foucaudeau, C. Ollier, A. W. Draney, T. Le Marchand, D. Cala-De Paepe, I. C. Felli, R. Pierattelli, S. Hiller, W. Bermel, G. Pintacuda, *Angew. Chem. Int. Ed.* **2019**, *58*, 2380–2384.
[41] A. Torosyan, T. Wiegand, M. Schledorn, D. Klose, P. Günthert, A. Böckmann, B. H. Meier, *Front. Mol. Biosci.* **2019**, *6*, 1–8.
[42] H. Van Melckebeke, C. Wasmer, A. Lange, A. B. Eiso, A. Loquet, A. Böckmann, B. H. Meier, *J. Am. Chem. Soc.* **2010**, *132*, 13765–13775.
[43] R. A. Crowther, N. A. Kiselev, B. Böttcher, J. A. Berriman, G. P. Borisova, V. Ose, P. Pumpens, *Cell* **1994**, *77*, 943–950.
[44] A. Y. Nazarenko, *J. Chem. Crystallogr.* **2019**, 1–7.
[45] D. Massiot, F. Fayon, M. Capron, I. King, S. Le Calvé, B. Alonso, J. -O Durand, B. Bujoli, Z. Gan, G. Hoatson, *Magn. Reson. Chem.* **2002**, *40*, 70–76.

Manuscript received: May 29, 2020
Accepted manuscript online: June 5, 2020
Version of record online: July 29, 2020